Available online at www.sciencedirect.com
ScienceDirect
Polymer 47 (2006) 7564–7571
polymer
www.elsevier.com/locate/polymer

Porous structure of crystalline polymers by exclusion effect of carbon dioxide

Yoshiaki Koga, Hiromu Saito*

Department of Organic and Polymer Materials Chemistry, Tokyo University of Agriculture and Technology, 2-24-16 Nakacho, Koganei-shi, Tokyo 184-8588, Japan

Received 19 June 2006; received in revised form 15 August 2006; accepted 20 August 2006
Available online 11 September 2006

Abstract

We investigated the morphology of high-density polyethylene (HDPE) and poly(vinylidene fluoride) (PVDF) crystallized under carbon dioxide (CO_2) by light scattering measurements and microscopic observations. The crystallization of HDPE was delayed and the ordering of the spherulite was smaller by dissolving CO_2 rather than air at ambient pressure. A fine-layered porous structure having a size of 500 nm was obtained in HDPE, while a large rod-like porous structure radiating in the spherulite was obtained in PVDF. Such a characteristic porous structure is attributed to the exclusion of CO_2 from the crystal growth front to the intercrystalline amorphous region and the growth of bubbles by the supersaturation of CO_2 in the constrained amorphous region. The exclusion effect is covered by the Keith–Padden theory through consideration of the self-diffusion in polymer–CO_2 systems; the exclusion and the growth of bubbles occur as lamellar stacks in HDPE whereas they occur as bundles of lamellar stacks in PVDF.

Keywords: Carbon dioxide; Crystallization; Porous structure

1. Introduction

Carbon dioxide (CO_2) can dissolve into polymers. In polymers, the dissolved CO_2 causes plasticizing effects such as depression of glass transition temperature and enhancement of chain mobility. Such plasticizing effects are expected to control crystalline morphology [1–3] and the rate of crystallization [4–9]. Spherulites were obtained by melt-crystallization of polypropylene under CO_2 after the CO_2 was dissolved at room temperature, while a mosaic crystalline texture consisting of regularly arranged long and straight lamellae was obtained by melt-crystallization after the CO_2 was dissolved at high temperature above the melting temperature, as an example see Ref. [3]. The crystallization rate of polymers, estimated by a high-pressure differential scanning calorimetry and infrared spectrometry, increases with increasing CO_2 pressure by dissolving CO_2 in poly(vinylidene fluoride) [4], polycarbonate [5], poly(ethylene terephthalate) [6,7], poly (ether ether ketone) [8], and isotactic polypropylene [9]. Such accelerated crystallization has been explained by the enhancement of the chain mobility for crystallization due to the plasticizing effect.

However, microscopically, the crystallization behavior of polymers under CO_2 is expected to be fundamentally different from that under air at ambient pressure. In the crystallization of polymers under CO_2, CO_2 should diffuse away from a crystal growth front, i.e., the exclusion should at least occur in the order of lamellar size. This situation is similar to that demonstrated in a mixture of a crystalline polymer and an amorphous one [10–17]. The result is complicated diffusion so that the crystallization kinetics and crystalline morphology differ from that under air at ambient pressure. Recently, we found that crystallization of polypropylene (PP) was delayed by the dissolution of CO_2; the delay in the crystallization was interpreted by the Hoffman–Lauritzen theory through consideration of the exclusion of CO_2 from the crystal growth front [18].

* Corresponding author. Tel./fax: +81 42 388 7294.
E-mail address: hsaitou@cc.tuat.ac.jp (H. Saito).

0032-3861/$ - see front matter © 2006 Elsevier Ltd. All rights reserved.
doi:10.1016/j.polymer.2006.08.052

In this paper, to understand the exclusion effect of CO_2 on crystallization kinetics and crystalline morphology, we investigate the isothermal crystallization of high-density polyethylene (HDPE) under CO_2 over a wide pressure range by time-resolved Hv light scattering using a high-pressure cell and characterize the morphology by analyzing the light scattering results and microscopic observations. The results are discussed on the basis of the Keith–Padden theory involving the exclusion effect of CO_2. The crystalline morphology of poly(vinylidene fluoride) (PVDF) obtained under CO_2 is also presented for deeper understanding of the exclusion effect of CO_2.

2. Experimental

The HDPE pellets used in this study were supplied by Mitsui Chemicals, Inc. (HZ1705J, $M_w = 67{,}000$). PVDF powder was supplied by Kureha Chemical Industry Co., Ltd. (KF1000, $M_w = 70{,}000$). In order to obtain a film specimen with a thickness of 50 μm, the HDPE pellets and PVDF powder were compression-molded between the two cover glasses at 190 °C and 200 °C for 5 min, respectively, and were then quickly quenched in a water bath.

In order to investigate the isothermal crystallization of HDPE under CO_2, a light scattering apparatus was installed above a specially designed high-pressure observation cell constructed of stainless steel with an inner volume of 20 mL (Taiatsu Techno Co. Ltd.), which was described in our previous paper [19]. Two sapphire glass windows were mounted on the cell. A film specimen (1.5 cm × 1.5 cm) was placed on the sapphire window positioned at the lower part of the cell. The temperature was raised to the desired melting temperature T_m to melt the crystallites. After the crystallites were melted, high-pressure CO_2 was injected into the vessel with a syringe pump (NP-KX-500J, Nihon Seimitsu Kagaku Co., Ltd.) and kept there for 1 h so that the CO_2 would dissolve into the specimen. The pressure proof of this cell is 20 MPa. After melting, the specimen was cooled to the desired crystallization temperature T_c; melt-crystallization occurred at T_c. A polarized He–Ne laser with a wavelength of 632.8 nm was applied vertically to the film specimen in the cell. The scattered light was passed through an analyzer and then onto a highly sensitive charge-coupled device (CCD) camera with a sensor of 512 × 512 pixel having dimensions of 13.3 × 8.8 mm (Princeton Instruments, Inc., TE/CDD-512-TKM-1). This sensor provides time-resolved measurement of two-dimensional angular distribution of scattered light with 512 one-dimensional data points in a time scale of 0.2 s. We employed Hv geometry in which the optical axis of the analyzer was set perpendicularly to that of the polarizer. The input data from the CCD camera was digitized by the ST-13X controller. The digitized data were stored in a personal computer for further analysis.

In order to obtain the crystallized specimen under high-pressure CO_2 above 20 MPa, a 50 mL stainless steel pressure vessel with a pressure proof of 50 MPa (Taiatsu Techno Co. Ltd.) was used. The inner diameter of the vessel is 45 mm and the outer diameter is 70 mm. The crystallized specimen was obtained under CO_2 by use of the method described above.

The crystallized specimen thus obtained was depressurized to ambient pressure and cooled to room temperature. The crystallized specimen was then observed under a polarized optical microscope (Olympus BH50) equipped with a sensitive tint plate having an optical path difference of 0.53 μm. Microscopic images of the specimen were recorded by a digital camera (Olympus DP11) and stored in a personal computer. The Hv light scattering measurement for the crystallized specimen was also performed under air at ambient pressure by using the CCD camera system described above.

The morphology of the crystallized specimens was also observed under a SEM (Hitachi S2100A). For observation, the specimen was fractured in liquid nitrogen and sputter-coated with platinum.

3. Results and discussion

Small spherulites, several micrometers in size, were obtained by cooling high-density polyethylene (HDPE) film to the crystallization temperature of 120 °C after dissolution of CO_2 at a temperature above the melting temperature. Since the spherulites were too small to discuss crystalline morphology based on observations by the polarized optical microscope, the crystallization kinetics and crystalline morphology obtained under CO_2 will be discussed in the following paragraphs in terms of Hv light scattering.

The Hv light scattering pattern from the HDPE spherulites was of a circular–symmetric type, i.e., there was no azimuthal angle dependence. This suggests that the optical axes of the crystals are randomly oriented in the spherulite. In this case, therefore, to discuss the kinetic aspect of the crystallization, it is convenient to employ the integrated scattering intensity in Hv mode, i.e., the invariant Q_{Hv} defined by [20–22]:

$$Q_{Hv} = \int_0^\infty I(q) q^2 \mathrm{d}q \tag{1}$$

where $I(q)$ is the intensity of the scattered light at the scattering vector q; $q = (4\pi/\lambda)\sin(\theta/2)$, λ and θ being the wavelength of the light and the scattering angle, respectively. Q_{Hv} is described by the mean square optical anisotropy δ:

$$Q_{Hv} \propto \langle \delta^2 \rangle = \Phi_s (\alpha_r - \alpha_t)^2 \tag{2}$$

where Φ_s is the volume fraction of the spherulites, and α_r and α_t are the radial and tangential polarizabilities of the spherulites, respectively. Hence, Q_{Hv} is expected to increase with an increasing volume fraction of the spherulites and then levels off when the spherulites are volume-filled [21,22].

Fig. 1 shows the time variation of invariants Q_{Hv} for HDPE crystallized at various CO_2 pressures at 120 °C. Q_{Hv} increases with time and levels off, as expected from Eq. (1), i.e., Φ_s increases and attains its maximum value when the spherulites fill the whole space. The crystallization period is 300 s under CO_2 at 15 MPa and is 150 s under CO_2 at 10 MPa, while it

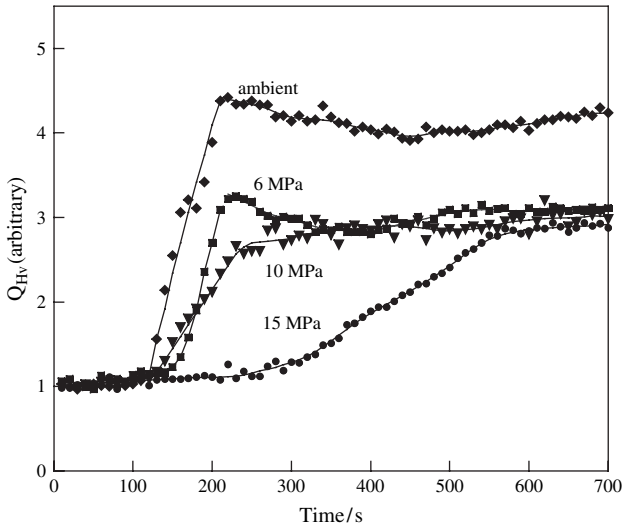

Fig. 1. Time variation of invariants Q_{Hv} for HDPE crystallized at 120 °C under CO_2 of various pressures.

is 90 s under air at ambient pressure, for instance. The results suggest that the crystallization of the HDPE is delayed by the dissolving CO_2.

According to the Hoffman–Lauritzen theory on polymer crystallization [23,24], the growth rate of crystallite G is given by:

$$G \propto \beta_g \exp\left(\frac{-K_g}{T_c \Delta T f}\right) \tag{3}$$

where β_g is the mobility term that describes the transportation rate of the crystallizable molecules at the growth front, T_c is the crystallization temperature, $\Delta T = T_m^\circ - T_c$ is the degree of supercooling (T_m° being the equilibrium melting temperature), f is the correction factor given by $2T_c/(T_m^\circ + T_c)$, and K_g is the nucleation constant. As demonstrated in our previous paper [18], the change in the growth rate with CO_2 pressure is not attributed to the change in K_g. Since the melting temperature of the HDPE was 134 °C and the change was little by absorbing CO_2, the change in the ΔT does not contribute to the change in the growth rate. Thus, the delay in crystallization under CO_2 might be ascribed to the decrease of β_g with an increase in the CO_2 pressure.

β_g is proportional to the diffusion coefficient in the secondary nucleation process. The crystal growth process in polymer is described as consisting of two elementary processes: the deposition of the first stem on the growth front (surface nucleation process) and the attachment of subsequent stems in the chain on the crystal surface (surface spreading process). We denote the diffusion coefficients in the surface nucleation process and the surface spreading process by D_M and D_S, respectively. In the neat crystalline polymer, it has been assumed that there is no distinction between D_M and D_S [23,24]. However, in the crystallization of polymers under CO_2, the situation should be different because of the exclusion of CO_2 from the crystal growth front, as for mixtures of a crystalline polymer and an amorphous one [10–17]. In other words, the two competitive processes should control diffusion in the secondary nucleation process in the crystallization of a HDPE–CO_2 system in which CO_2 is dissolved in HDPE: the attachment of the crystalline polymer onto the crystal surface and the exclusion of CO_2 from the surface. This competitive situation can be characterized by mutual diffusion. On the other hand, surface spreading may be controlled by the rate of pull-out of residual segments in the crystalline chain from the melt near the growth front. This can be characterized as the self-diffusion of polymers plasticized by CO_2. Since the self-diffusion of polymers usually increases with an increase in the CO_2 pressure and it is opposite to the experimental results, the β_g might be governed by mutual diffusion.

The mutual-diffusion coefficient in the HDPE–CO_2 system may be given by a phenomenological equation for polymer mixtures suggested by Alfonso and Russell [13]:

$$D_M \propto (1 - \phi_{CO_2}) \frac{D_{HDPE} D_{CO_2}}{D_{HDPE} + D_{CO_2}} \tag{4}$$

where ϕ is the volume fraction and D is the diffusion coefficient for HDPE and CO_2. Eq. (4) claims that the mutual diffusion is generally governed by the slower moiety at low ϕ_{CO_2}.

The calculated results for D_M obtained from Eq. (4) are shown in Fig. 2 as a function of ϕ_{CO_2} and pressure P. Here, ϕ_{CO_2} is proportional to the pressure of CO_2 and the value of ϕ_{CO_2} is calculated from the data of CO_2 dissolved in HDPE obtained by Sato et al. [25]. Because D_{CO_2} has an order of magnitude of 10^{-1} cm^2/s and D_{HDPE} has one of 10^{-8} cm^2/s, we have assumed $D_{CO_2}/D_{HDPE} = 10^7$. D_M decreases with increasing ϕ_{CO_2} as the pressure of CO_2 increases. Thus, the decrease in β_g with pressure might be attributed to the decrease in D_M caused by the exclusion effect of CO_2. The decrease in β_g by the exclusion effect of CO_2 might cause the delay of the crystallization by the dissolving CO_2.

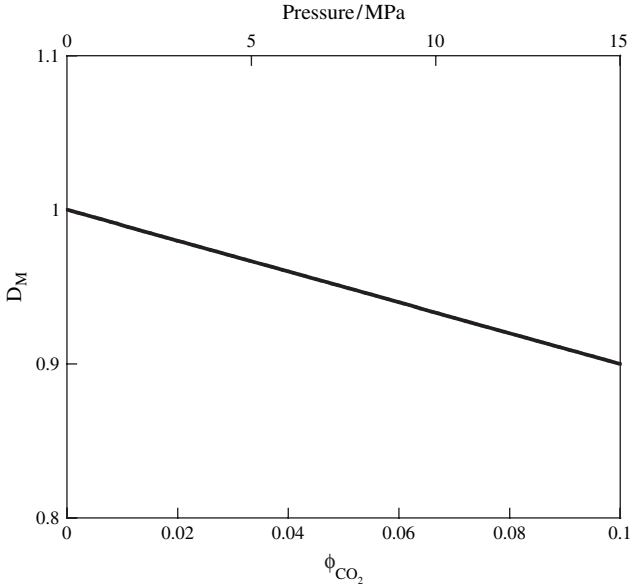

Fig. 2. Calculated curve of mutual-diffusion coefficient D_M in HDPE–CO_2 system as a function of CO_2 pressure.

As shown in Fig. 1, the invariant Q_{Hv} of the crystallized HDPE obtained under CO_2 is much smaller than that under air at ambient pressure. According to Eq. (2), Q_{Hv} is related to the polarizability difference $(\alpha_r - \alpha_t)$. Since $(\alpha_r - \alpha_t)$ is ascribed to the intrinsic anisotropy of the crystalline region and the orientation function for the optical axis of the crystalline region, the small value of Q_{Hv} is caused by the low orientation of the optical axis in the spherulite. This suggests that the ordering in the spherulite obtained under CO_2 is much smaller than that under air at ambient pressure.

As demonstrated before, the Hv light scattering pattern was circular and symmetric. In this case, light scattering intensity I_{Hv} is described by an assumption of random orientation [26]:

$$I_{Hv} \propto \langle \delta \rangle^2 \int_0^\infty f(r) \frac{\sin qr}{qr} 4\pi r^2 dr \tag{5}$$

where *f(r)* is the correlation function of orientation fluctuation in an optical axis at separation distance *r*. Assuming that *f(r)* is given by the exponential correlation function:

$$f(r) = \exp(-r/a) \tag{6}$$

where *a* is the orientation correlation distance, the angular dependence of I_{Hv} is described by the Debye–Bueche type scattering function [20,27–29]:

$$I_{Hv}^{-1/2} = \frac{1}{A} + \frac{a^2}{A} q^2 \tag{7}$$

where *A* is constant and *a* is the orientation correlation distance. The orientation correlation distance *a* is described by [29]:

$$a = \frac{2d}{3\varepsilon^2} \tag{8}$$

where *d* is the size of lamellar stack. ε is the average angle between the optical axes of neighboring lamellar stacks and is a parameter describing the degree of disorder for the arrangement of lamellar stacks [30]. Hence, we can employ the orientation correlation distance *a* as a measure of the ordering in the spherulite.

As shown in Fig. 3, the plot of $I_{Hv}^{-1/2}$ vs q^2 yielded straight lines as expected from Eq. (7). The orientation correlation distance *a* can be obtained from the slope and the intercept in the plots of $I_{Hv}^{-1/2}$ vs q^2. The pressure dependence of *a* thus obtained is shown in Fig. 4. The value of *a* of crystallized HDPE obtained under CO_2 is much smaller than that obtained under air at ambient pressure. The results support the change of the ordering in the spherulite by dissolving CO_2, i.e., the ordering in the spherulite obtained under CO_2 is much smaller than that obtained under air at ambient pressure. This may be attributed to the exclusion of CO_2 from the crystal growth front to the amorphous region, as for mixtures of a crystalline polymer and an amorphous one [10–17].

Figs. 5 and 6 are SEM micrographs of HDPE obtained by crystallization at 120 °C under various pressures of CO_2. A layered porous structure having a size of 500 nm is seen,

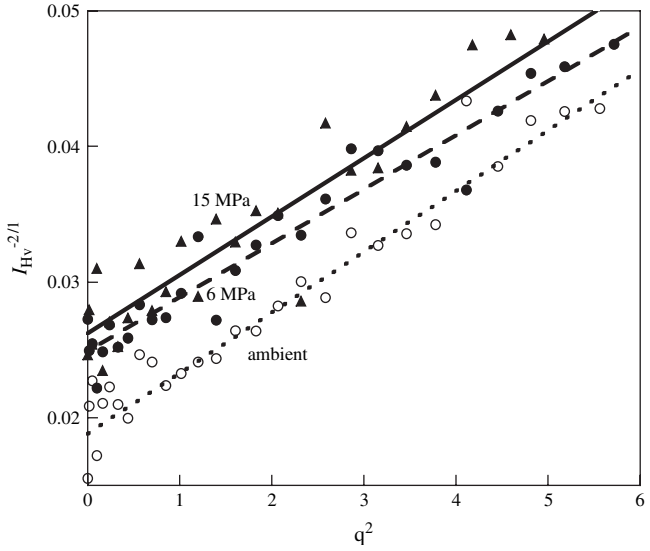

Fig. 3. Debye–Bueche plots of Hv scattering intensity for HDPE crystallized at 120 °C under CO_2 of various pressures.

and the pore is enclosed by an interconnected phase. The pore size is much smaller than that obtained by conventional foaming of melt HDPE in which the pore size is of several 10 μm [31]. This structure is similar to that obtained by extracting the amorphous phase of HDPE using hot xylene or fuming nitric acid, i.e., the pore is obtained by extracting the amorphous phase and is enclosed by the interconnected lamellar stacks remaining after the extraction [32,33]. Since the pore size is larger than the next-neighbor distance of the lamellae in which the size is of several nm [34], the porous structure shown in Figs. 5 and 6 might consist of layered pores enclosed by interconnected lamellar stacks. The pore size increases with an increase in CO_2 pressure at low CO_2

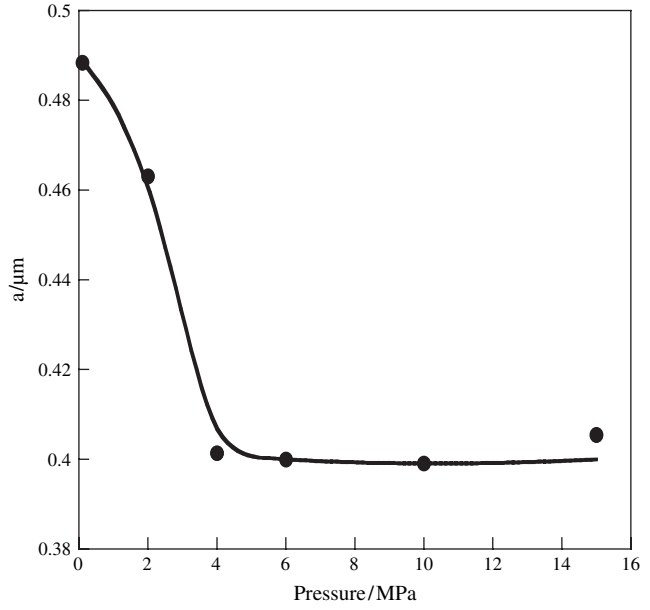

Fig. 4. Orientation correlation distance *a* as a function of CO_2 pressure.

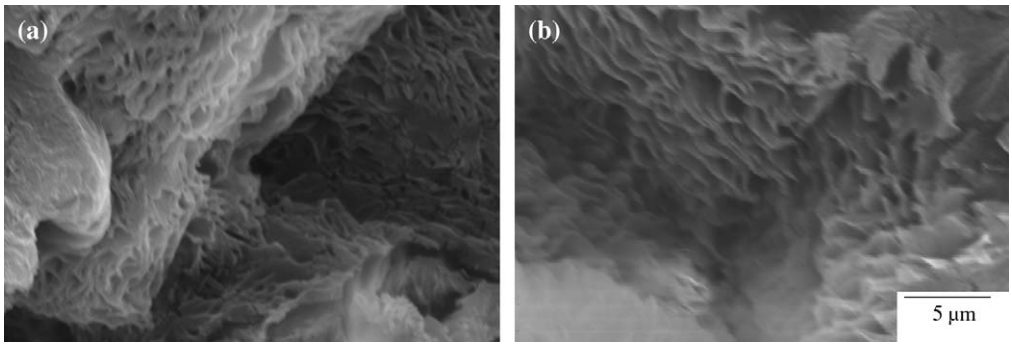

Fig. 5. SEM micrograph of HDPE crystallized at 120 °C under CO_2 of various pressures: (a) 3 MPa and (b) 30 MPa.

pressures below 5 MPa (Fig. 5(a)), but the change with CO_2 pressure becomes slight at higher pressures (Figs. 5(b) and 6). This result corresponds to that of the ordering in the spherulite demonstrated in Fig. 4, suggesting that pore development is caused by the exclusion of CO_2.

There might be two possibilities for the development of the pore: one is the foam that develops in the amorphous region between the lamellar stacks during depressurization after crystallization; the other is exclusion of CO_2 during the crystallization before the depressurization. If the former is the case, changing the depressurization rate will change the shape and size of the pore. The result in Fig. 6 contradicts this, i.e., pore size and shape were not changed when the depressurization rate was changed. Thus, the latter possibility seems to be more realistic, that is, the pore is attributed to the exclusion of CO_2 during the crystallization before depressurization.

Fig. 7 is a schematic illustration of the exclusion of CO_2 and the development of the pore during the crystallization of HDPE under CO_2. CO_2 is dissolved in HDPE during the melt state (Fig. 7(a)). When HDPE is cooled to the crystallization temperature below the melting temperature, crystallization occurs. Since the CO_2 cannot be dissolved in the crystals, CO_2 is excluded from the growth front of the crystals to the intercrystalline amorphous region (Fig. 7(b)). Due to the exclusion, the concentration of CO_2 in the intercrystalline amorphous region becomes greater than that in the melt state (Fig. 7(c)). When the concentration of the CO_2 in the amorphous region exceeds supersaturation, bubbles nucleate and grow, resulting in a porous material as in the case of foaming [31,35–42] (Fig. 7(d)). When the exclusion occurs in a scale of lamellar stacks, bubbles grow in the amorphous region between the lamellar stacks. Because of the constraint by the neighboring lamellae, the growth of bubbles is stopped within the amorphous region between the lamellar stacks. Thus, the structure around the pore is similar to that of the lamellar stack, as shown in Figs. 5 and 6, while a large amount of porous material in a spherical shape is obtained in the area without constraint by the foaming amorphous polymers.

The exclusion of CO_2 can be quantitatively discussed in terms of the parameter δ suggested by Keith and Padden [10,11]:

$$\delta = \frac{D}{G} \tag{9}$$

where δ is the distance in which the non-crystalline component can be excluded from the crystal growth front, D is the diffusion coefficient of the non-crystalline component (CO_2), and G is the growth rate of the crystalline polymer. The diffusion coefficient of the non-crystalline component D is expressed by the self-diffusion of CO_2 which describes the diffusion of CO_2 in molten HDPE. The self-diffusion coefficient may be given by [43,44]:

$$D \propto \left(D_{\mathrm{HDPE}}\phi_{\mathrm{HDPE}} + D_{\mathrm{CO_2}}\phi_{\mathrm{CO_2}}\right) \tag{10}$$

The calculated result for D obtained from Eq. (10) is shown in Fig. 8 as a function of CO_2 pressure. D increases steeply at low CO_2 pressures below 2 MPa and then increases gradually with increasing CO_2 pressure. Since the change in D is small with CO_2 pressures above 5 MPa, the changes in pore size and

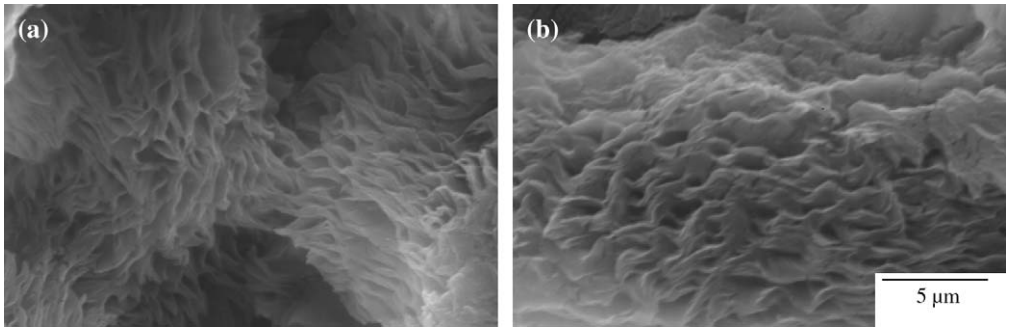

Fig. 6. SEM micrograph of HDPE obtained at various depressurization rates after crystallization at 120 °C under CO_2 of 15 MPa: (a) 0.5 MPa/min and (b) 5 MPa/s.

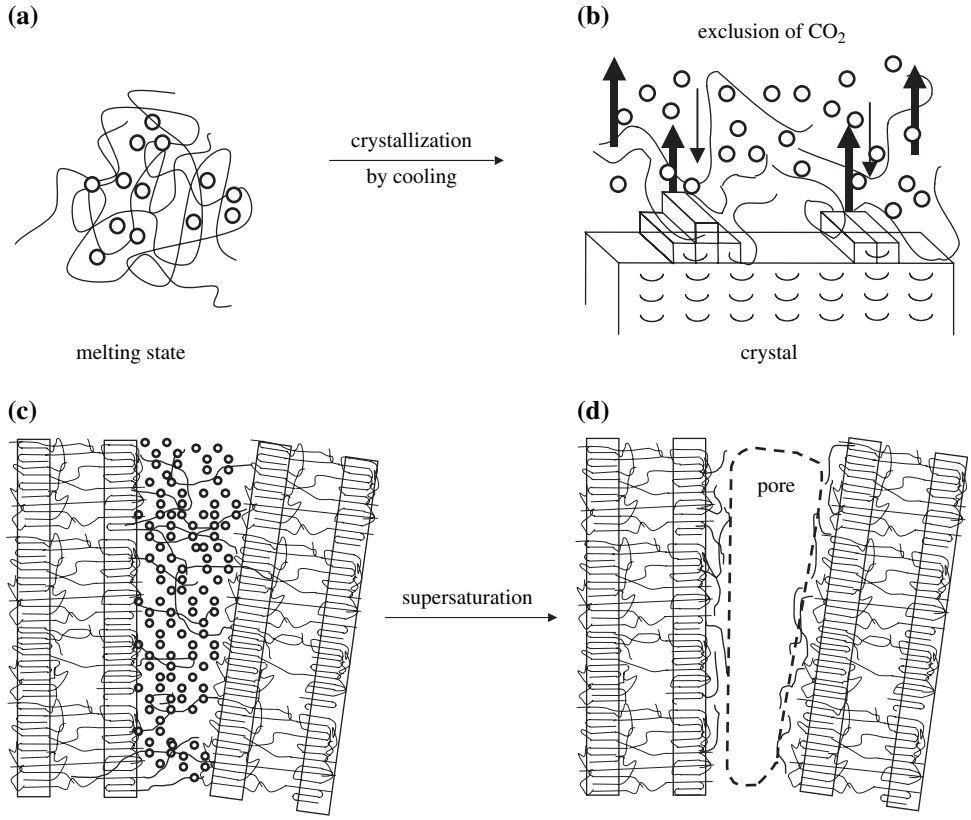

Fig. 7. Schematic of pore development during crystallization under CO_2.

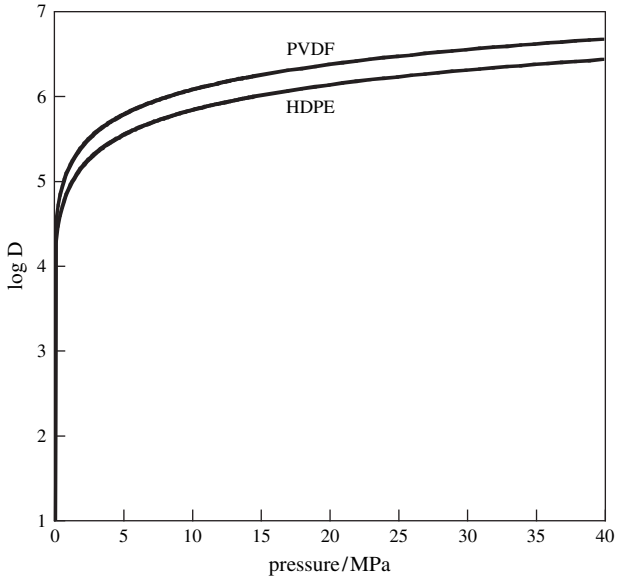

Fig. 8. Calculated curve of diffusion coefficient for non-crystalline component D in HDPE–CO_2 and PVDF–CO_2 systems as a function of CO_2 pressure.

the ordering in the spherulite are slight at high CO_2 pressures above 5 MPa, as shown in Figs. 4–6. Since the distance of the exclusion δ increases as D increases, pore size increases and the ordering in the spherulite decreases as δ increases.

Fig. 9 shows SEM micrographs of HDPE obtained under CO_2 by isothermal crystallization at 120 °C and quenching with a water bath from the melt state. The pore size of the quenched specimen is smaller than that obtained by isothermal crystallization at a high temperature. The temperature of crystallization during the quenching is lower than that of isothermal crystallization. According to Eq. (9), it is expected that the lower the temperature of crystallization, the smaller is D and the larger is G, then the smaller could be the distance of the exclusion δ. This might explain the small pore in HDPE obtained by quenching under CO_2. The result supports the exclusion of CO_2 during crystallization under CO_2.

It is well known that the dissolution of CO_2 in PVDF is larger than that in HDPE [44,45]. The calculated results for D of PVDF obtained from Eq. (10) are also shown in Fig. 8 as a function of CO_2 pressure P. The D of PVDF is larger than that of HDPE. Hence, it is expected that the distance of the exclusion δ in PVDF is larger than that in HDPE.

Fig. 10 shows the polarized optical micrographs of PVDF crystallized at 150 °C under various CO_2 pressures. Compact spherulites having a clear Maltese cross pattern and banding pattern are obtained by crystallization under air at ambient pressure (Fig. 10(a)). Similarly, compact spherulites are developed under CO_2 at 15 MPa (Fig. 10(b)). However, the Maltese cross pattern is more diffuse and the period of the banding is longer compared to those obtained under air at ambient pressure. The diffuse Maltese cross pattern is attributed to the randomness of the orientation of the lamellar stacks. As the CO_2 pressure increases, the Maltese cross pattern becomes more diffuse, and the mottling of the regions where no light

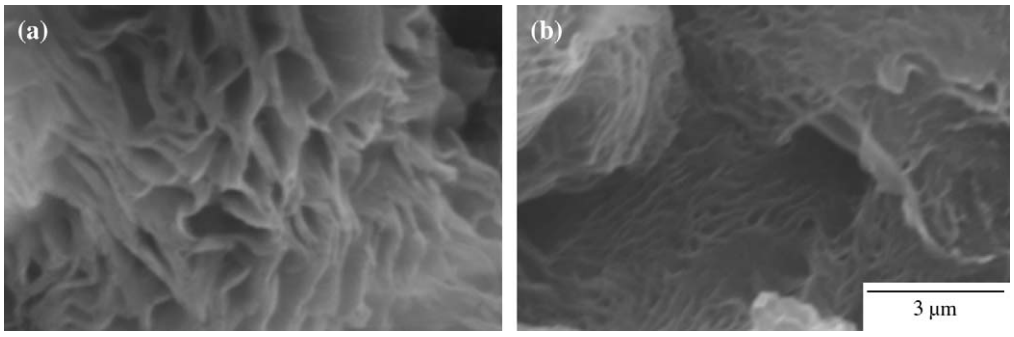

Fig. 9. SEM micrograph of HDPE crystallized under CO_2 of 15 MPa: (a) isothermal crystallization at 120 °C and (b) quenching from 150 °C in water bath.

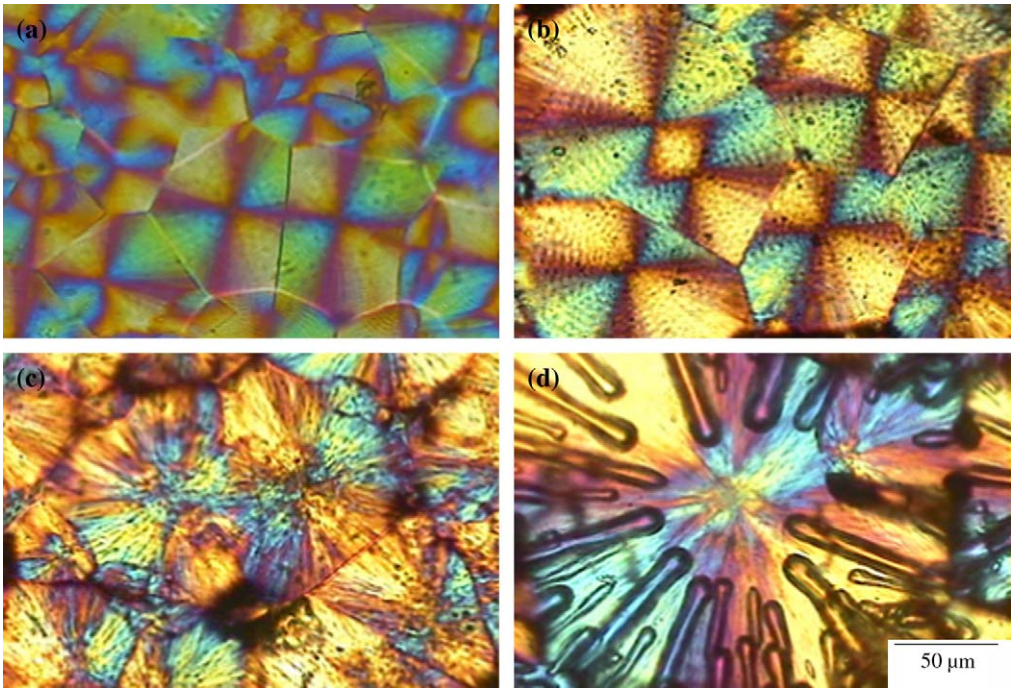

Fig. 10. Polarized optical micrograph of PVDF crystallized at 150 °C under CO_2 of various pressures: (a) under air at ambient pressure, (b) 15 MPa, (c) 25 MPa and (d) 40 MPa.

is transmitted appears (Fig. 10(c)). When PVDF is crystallized at CO_2 pressures above 35 MPa, large rod-like pores having sizes of 10 μm in diameter are obtained within the spherulite (Fig. 10(d)). The pores are arranged radially from the center of the spherulites. The pore size is much larger than that obtained in HDPE. The difference might be caused by the different D calculated from Fig. 8. Such a characteristic porous structure might be due to the exclusion of CO_2 from the growth front of the bundle of lamellar stacks during spherulite growth. These results also support the exclusion effect of CO_2 on the crystalline morphology of polymers.

4. Conclusion

We found that a fine-layered porous structure was obtained in HDPE and a large rod-like porous structure radiating in the spherulite was obtained in PVDF by crystallization under CO_2. Such a characteristic porous structure is attributed to the exclusion of CO_2 from the crystal growth front to the inter-crystalline amorphous region and the growth of bubbles by the supersaturation of CO_2 in the constrained amorphous region. Due to the exclusion, the crystallization rate is delayed and ordering in the spherulite decreases. The exclusion of CO_2 and the development of pores can be qualitatively explained by the Keith–Padden theory through consideration of self-diffusion in polymer–CO_2 systems.

References

[1] Handa YP, Roovers J, Wang F. Macromolecules 1994;27:5511.
[2] Handa YP, Zhang Z, Wong B. Macromolecules 1997;30:8499.
[3] Teramoto G, Oda T, Saito H, Sano H, Fujita Y. J Polym Sci Part B Polym Phys 2004;42:2738.
[4] Chiou JS, Barlow JW, Paul DR. J Appl Polym Sci 1985;30:3911.
[5] Beckman E, Porter RS. J Polym Sci Part B Polym Phys 1987;25:1511.

[6] Mizoguchi K, Hirose T, Naito Y, Kamiya Y. Polymer 1987;28:1298.
[7] Lambert SM, Paulaitis ME. J Supercrit Fluids 1991;4:15.
[8] Zhang Z, Handa YP. J Polym Sci Part B Polym Phys 2001;39:1505.
[9] Takada M, Tanigaki M, Ohshima M. Polym Eng Sci 2001;41:1938.
[10] Keith HD, Padden Jr FJ. J Appl Phys 1963;34:2409.
[11] Keith HD, Padden Jr FJ. J Appl Phys 1964;35:1270.
[12] Stein RS, Khambatta FB, Warner FP, Russell T, Escala A, Balizer E. J Polym Sci Polym Symp 1978;63:313.
[13] Alfonso GC, Russell TP. Macromolecules 1986;19:1143.
[14] Stein RS. Pure Appl Chem 1991;63:941.
[15] Saito H, Okada T, Hamane T, Inoue T. Macromolecules 1991;24:4446.
[16] Hudson SD, Davis DD, Lovinger AJ. Macromolecules 1992;25:1759.
[17] Okada T, Saito H, Inoue T. Polymer 1994;35:5699.
[18] Oda T, Saito H. J Polym Sci Part B Polym Phys 2004;42:1565.
[19] Hatanaka M, Saito H. Macromolecules 2004;37:7358.
[20] Koberstein J, Russell TP, Stein RS. J Polym Sci Polym Phys Ed 1979;17:1719.
[21] Lee CH, Saito H, Inoue T. Macromolecules 1993;26:6566.
[22] Tsuburaya M, Saito H. Polymer 2004;45:1027.
[23] Lauritzen JI, Hoffman JD. J Appl Phys 1973;44:4340.
[24] Hoffman JI. Polymer 1983;24:3.
[25] Sato Y, Fujisawa K, Takikawa T, Sumarno Takishima S, Masuoka H. Fluid Phase Equilib 1999;162:261.
[26] Stein RS, Wilson PR. J Appl Phys 1963;33:1914.
[27] Debye P, Bueche AM. J Appl Phys 1949;20:518.
[28] Debye P, Anderson Jr HR, Brumberger H. J Appl Phys 1957;128:679.
[29] Stein RS, Stidham SN. J Appl Phys 1964;35:42.
[30] Stein RS, Chu W. J Polym Sci Part A-2 1970;8:1137.
[31] Klempner D, Frisch KC, editors. Handbook of polymeric foams and foam technology. Munich: Hanser Publishers; 1991.
[32] Shimomura K, Murakami S, Katayama K. Makromol Chem Rapid Commun 1982;3:199.
[33] Winram MM, Grubb DT, Keller A. J Mater Sci 1987;13:791.
[34] Fukuoka M, Aya T, Saito H, Ichihara S, Sano H. Polym J 2006;38:542.
[35] Khemani KC, editor. Polymeric foams, science and technology. Washington, DC: American Chemical Society; 1997.
[36] Lee ST, Ramesh NS, editors. Polymeric foams, mechanisms and materials. Boca Raton: CRC Press; 2004.
[37] Kumar V, Suh NP. Polym Eng Sci 1990;30:1323.
[38] Goel SK, Beckman EJ. Polym Eng Sci 1994;34:1137.
[39] Parks LK, Beckman EJ. Polym Eng Sci 1996;36:2417.
[40] Arora KA, Lesser AJ, McCarthy TJ. Macromolecules 1998;31:4614.
[41] Stafford CM, Russell TP, McCarthy TJ. Macromolecules 1999;32:7610.
[42] Krause B, Mettinkhof R, van der Vegt NFA, Wessling M. Macromolecules 2001;34:874.
[43] Brochard F, Jouffroy J, Levinson P. Macromolecules 1983;16:1638.
[44] Flory G, Cohen C. J Polym Sci Part B Polym Phys 1987;25:2027.
[45] Briscoe BJ, Lorge O, Wajs A, Dang P. J Polym Sci Part B Polym Phys 1998;36:2435.